RESEARCH ARTICLE

Key Points:
- WRF-SBM was used to simulate the landfalling Typhoon Saomai (2006)
- The aerosol concentration affects the structure, intensity, and precipitation of the typhoon
- More aerosols weaken the typhoon's intensity with increased rain rate in the outer rainbands

Correspondence to:
B. Chen and J. Ming,
bjchen@nju.edu.cn;
jming@nju.edu.cn

Aerosol Impacts on the Structure, Intensity, and Precipitation of the Landfalling Typhoon Saomai (2006)

Yi Qu[1], Baojun Chen[1] (iD), Jie Ming[1], Barry H. Lynn[2] (iD), and Ming-Jen Yang[3]

[1]Key Laboratory of Mesoscale Severe Weather/MOE, and School of Atmospheric Sciences, Nanjing University, Nanjing, China, [2]Department of Atmospheric Sciences, Hebrew University of Jerusalem, Jerusalem, Israel, [3]Department of Atmospheric Sciences, National Taiwan University, Taipei, Taiwan

Abstract Typhoon Saomai (2006) was simulated using the Weather Research and Forecasting (WRF) model with explicit spectral bin microphysics to investigate the effects of aerosol from mainland China on the intensity, structure, and precipitation of the landfalling storm. MAR (maritime), MIX (semicontinental), and CON (continental) experiments were conducted with different initial aerosol concentrations. Varying aerosol concentrations had little influence on the storm track but resulted in pronounced deviations in intensity and structures. The experiment with a high initial aerosol concentration showed invigorated convection at the periphery of the tropical cyclone (TC), which interfered with the reformation of the eyewall, leading to TC weakening. The minimum pressures in the CON and MIX experiments were increased by more than 30 hPa and 14.6 hPa, and their maximum wind speeds were 20 m s^{-1} and 13 m s^{-1} weaker than that in the MAR experiment, respectively. The rain rates in the MIX and CON experiments were 16.6% and 56.2% greater than that in the MAR run, with the differences mainly occurring in the outer rainbands. These results indicate that the aerosol concentration substantially affects the spatial distributions of cloud hydrometeors and rainfall. The increase of rainfall was triggered by an increase in the melting of graupel and cloud droplets collected by raindrops. Similarly, the graupel melting process also enhanced in the outer rainbands with increasing aerosol. Furthermore, a positive microphysics feedback associated with the rainwater in the outer rainbands played an important role in increasing the rain rate in more aerosol scenarios.

1. Introduction

Typhoons are one of the major natural disasters that occur in the coastal and some inland regions of China (Yu, 2015). Well-known factors affecting typhoon intensity include heat and moisture fluxes, which in turn are determined by the sea surface temperature (SST) and wind shear (e.g., Anthes, 1982; Emanuel, 2005; Khain, 1984). Landfalling typhoons are notorious for causing huge economic losses as well as death and injuries. For example, Typhoon Saomai (2006) affected 6,655,000 people in the Zhejiang, Fujian, and Jiangxi provinces, and approximately 483 people were killed by the storm. The economic losses in these provinces reached 196.5 billion yuan (U.S. $24.65 billion) (Zhang et al., 2009). In recent years, many improvements have been made in tropical cyclone (TC) forecasting, owing to advancements in observational technologies and numerical modeling. However, the operational intensity forecasts are considerably less accurate than the track forecasts (DeMaria et al., 2005). The prediction of typhoon intensities and structures remains a challenge. Uncertainty in the parameterization of cloud microphysics creates a large bias in numerical forecasts, especially for the forecasts of the intensity, gale force winds, and rainfall of a typhoon. It is believed that improving the microphysics parameterization in the forecast models is necessary for the advancement (Duan et al., 2012; Fritsch & Carbone, 2004). A comparison of the microphysical processes and predicted hydrometeor distributions between the model simulations and observations is essential (Stoelinga et al., 2003).

Over recent decades, aerosol particles have been found to serve as cloud condensation nuclei (CCN) or ice nuclei (IN), which can substantially affect the microphysics, rate of latent heat release, dynamics, and precipitation amount of a cloud. These influences depend on the concentrations of CCN, as well as the environmental conditions (Khain, 2009; Tao et al., 2012). On the one hand, some observations suggest that elevated aerosol can affect TC development via their influences on the microphysics of TC clouds (Jenkins & Pratt, 2008; Jenkins et al., 2008; Lau & Kim, 2007). Evan et al. (2011) used a combination of observational, reanalysis,
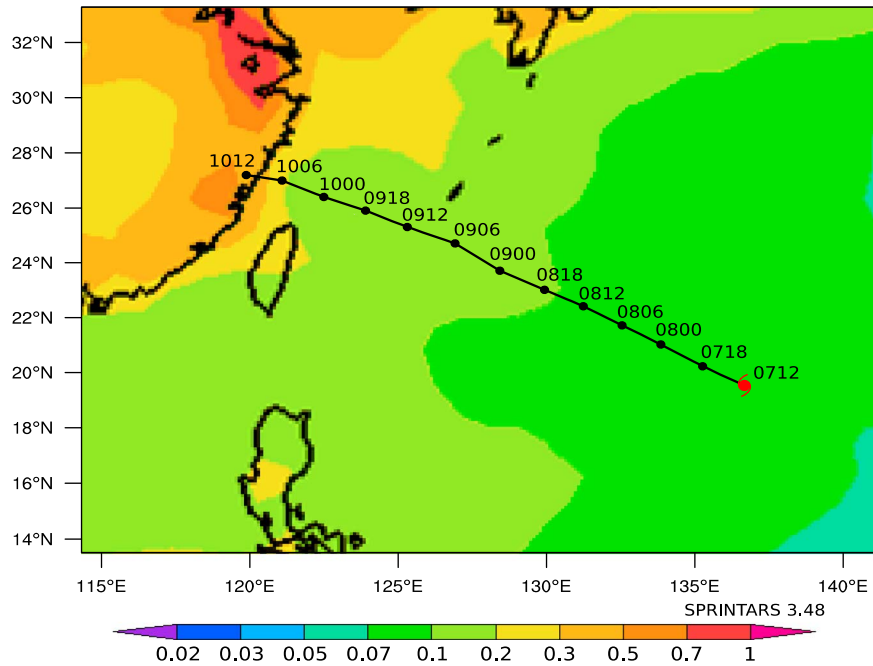
Figure 1. Monthly mean aerosol optical depth (AOD) at 550 nm in August 2006, given by the SPRINTARS (Spectral Radiation-Transport Model for Aerosol Species) model (http://sprintars.riam.kyushu-u.ac.jp/archive.html). The 6-hourly best track of Typhoon Saomai from the Joint Typhoon Warning Center (JTWC) is also shown.

and model data to demonstrate that the anomalous circulation in Arabian Sea was forced by anthropogenic aerosol. This work discovered that aerosol in the Arabian Sea decreased the basin-wide vertical wind shear, creating more favorable conditions for TC intensification. On the other hand, simulations show that high concentrations of CCN can substantially affect the TC intensity and structure (Cotton et al., 2007;
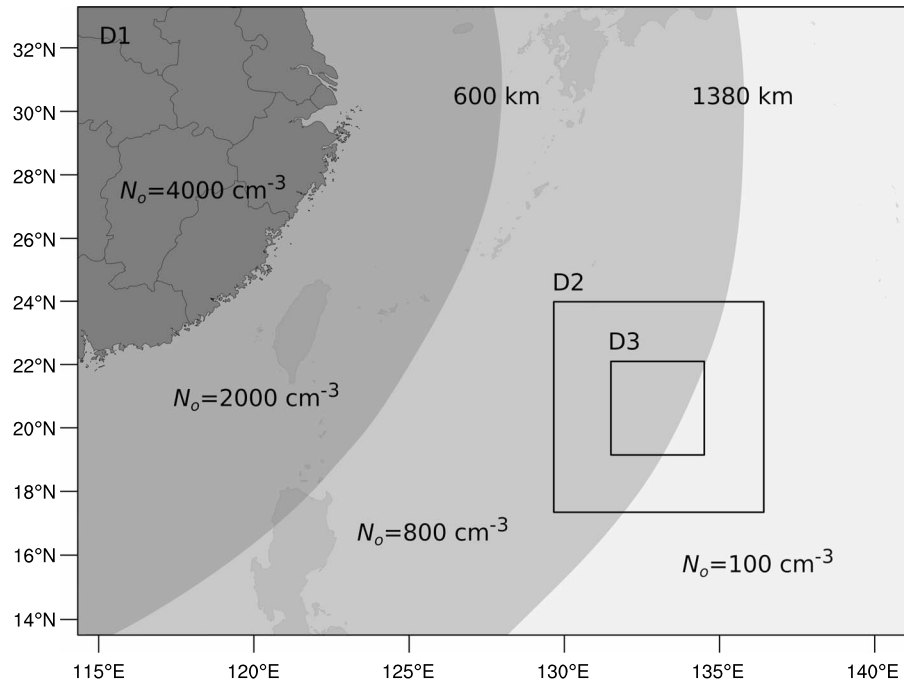

Figure 2. The initial position of the nested domains used for the WRF-SBM simulations: domain 1 (D1), with 12 km grid spacing; domain 2 (D2), with 4 km grid spacing; and domain 3 (D3), with 1.33 km grid spacing. D2 and D3 are automatic vortex-following moving nest grids. N_o represents the measured constant determining the number of condensation of aerosol particles. The 600 km and 1380 km are the distances from the coastline to the boundaries of the aerosol particles in the MIX simulation.
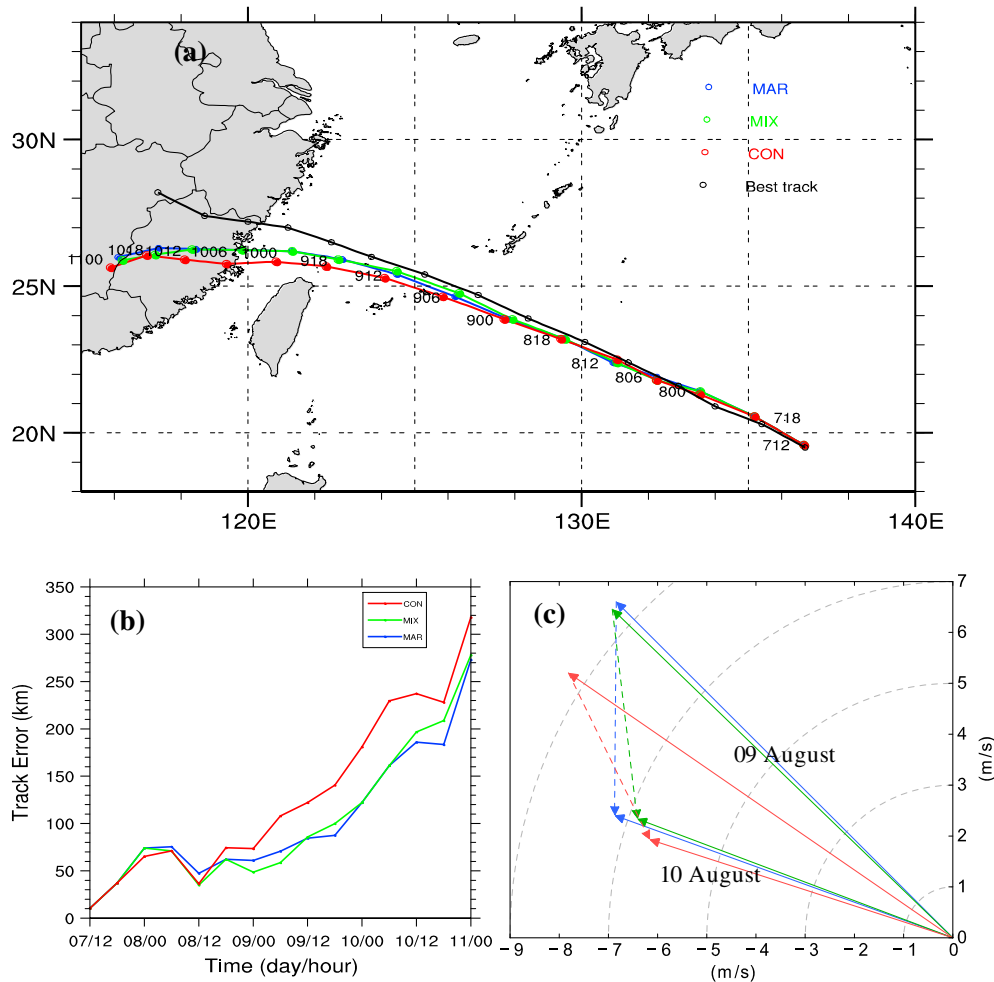
Figure 3. (a) The simulated tracks of Saomai in the three experiments and the best track (black line) from the JTWC from 1200 UTC on 7 August to 0000 UTC on 11 August. (b) The track errors of the three simulations in comparison with the best track. (c) The solid arrows are velocity vectors averaged over time- (6 h) and tropospheric-averaged steering flows of Typhoon Saomai at 0600 to 1200 UTC on 9 August and 0600 to 1200 UTC on 10 August, and the dashed arrows are the difference vectors: MAR (blue), MIX (green), and CON (red).

Hazra et al., 2013; Khain et al., 2010; Rosenfeld et al., 2011). The impact of CCNs on the TC intensity depends on the time when CCNs are transported to the outer rainbands, the intensity, and the lifecycle stages of the convection over the outer rainbands (Krall & Cottom, 2012). Khain, BenMoshe, and Pokrovsky (2008) and Khain et al. (2010) simulated the landfalling Hurricane Katrina (2005) using the explicit spectral bin microphysics (SBM) scheme in the Weather Research and Forecasting (WRF) model. They found that the higher concentrations in the semicontinental case (maritime-continental (MAR-CON)) led to a weaker storm. The minimum pressure changed by ~15 hPa, and the lightning activity was increased. They proposed that seeding TCs with pollution-sized aerosol particles could produce more small cloud droplets, reducing collision and coalescence, and possibly inhibiting further intensification of the TCs. Rosenfeld et al. (2012) showed that CCNs could weaken warm rain processes but would strengthen cold rain processes. They indicated that CCNs could decrease the intensities of TCs by enhancing convection in their outer rainbands and weakening the convection in the eyewall. Additionally, the increased CCNs could change the size distribution of the cloud droplets, which determined the precipitation-formation processes (Rosenfeld et al., 2008). Krall and Cottom (2012) used the Regional Atmospheric Modeling System with an advanced two-moment bin-emulating microphysics scheme to show that precipitation was reduced due to the suppressed collisions and coalescences that occurred soon after the ingestion of enhanced CCN, but more precipitations were produced afterward. Hazra et al. (2013) investigated two TCs over the Bay of Bengal using a two-moment mixed-phase bulk cloud microphysics scheme and found that regardless of whether the TC was intense
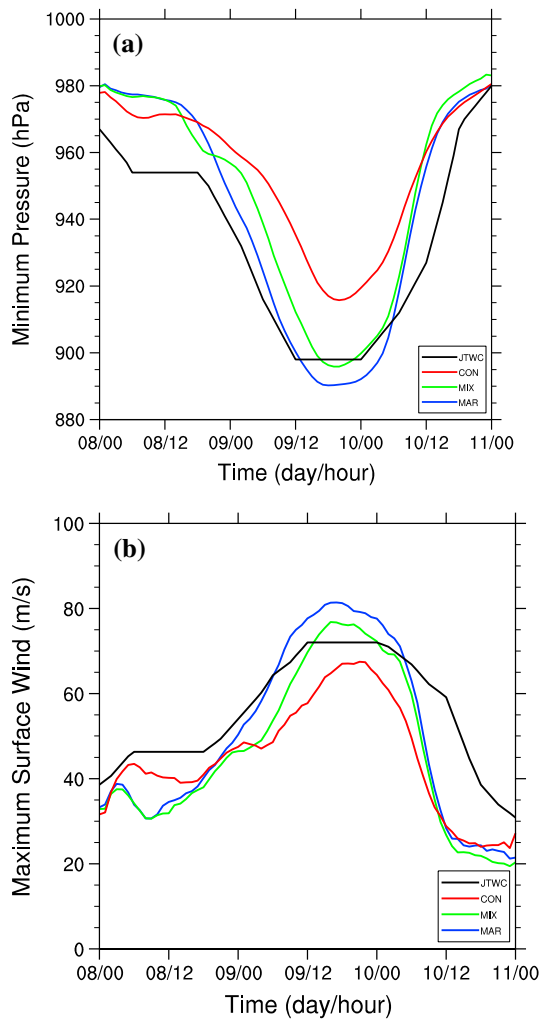
Figure 4. Time series of the intensity of Typhoon Saomai from three simulation experiments and the JTWC: (a) minimum central pressure (b) maximum surface velocity on the finest grid for the MAR (blue line), MIX (green line), and CON (red line) simulations.

(the first case) or weak (the second case), an increased CCN concentration led to a weakened storm and a different precipitation efficiency. In addition, different approaches of microphysical modeling showed various results (Khain et al., 2016; Ming et al., 2012). The microphysical structures of the clouds in simulated TCs were sensitive to the microphysical schemes used in the model.

In general, there are two main approaches to describe the cloud microphysical properties and processes in the model: bulk microphysical parameterization schemes (e.g., Fierro et al., 2007; Kessler, 1969; Thompson et al., 2006; Zhang et al., 2007; Zhang et al., 2009) and explicit bin schemes (e.g., Fan et al., 2009; Fan et al., 2012; Fan et al., 2013; Igel & van den Heever, 2014; Iguchi et al., 2014; Khain et al., 2010, 2015; Lynn et al., 2016; Tao et al., 2007; Yin et al., 2000). In bulk schemes, the exponential Marshall-Palmer or gamma distribution is used to describe the shape of the size distribution functions. Due to the simplified size distributions in this case, the computation of bulk schemes is efficient and therefore more popular. However, bulk schemes are much less sensitive to aerosol than SBM scheme (Khain et al., 2015; Khain et al., 2016). The microphysical details in the bulk scheme are not as precise as that in the SBM scheme. Fan et al. (2012) used the WRF model with different microphysical schemes to study the indirect aerosol effects in the warm and cold seasons in Southeast China. They found that compared with SBM, the bulk schemes generated much higher cloud droplet numbers and the opposite CCN effects on convection and heavy rain. Moreover, Lynn et al. (2016) applied the WRF-SBM scheme to simulate Hurricane Irene (2011), and they successfully analyzed the reason why the time of minimum pressure occurred approximately 40 h later than the time of maximum speed. Based on their work, Khain et al. (2016) applied several bulk parameterization schemes versus the SBM scheme to examine the sensitivity of hurricane simulations to aerosol and the choice of microphysical schemes. They found that the bulk schemes could not predict the time differences between the maximum wind and minimum pressures.

Asia is a primary source of emissions of diverse species of aerosol from both anthropogenic and natural origins (Li et al., 2016). Wang et al. (2014) demonstrated that the increasing aerosol from Southeast China probably inhibited the development of TCs. The bulk parameterization schemes have been used to examine the effects of aerosol on the Western Pacific TCs (e.g., Jiang et al., 2016; Li et al., 2008; Zhang et al., 2007). However, few studies have examined the microphysical effects of the aerosol by quantitatively considering the microphysical processes using the SBM scheme. Indirect aerosol forcings on precipitation could be evaluated by means of WRF coupled with the SBM scheme (Khain et al., 2004). This study aims to investigate and quantify the influence of aerosol distributions and concentrations on the storm track, intensity, structures, and precipitation of Typhoon Saomai (2006). Section 2 includes the model setup. Section 3 presents the simulation results and discussion and shows the microphysical mechanisms for the changes in TC intensity and structure. The summary and conclusions are given in section 4.

2. Model and Experimental Design

Figure 1 shows the observed 6-hourly track of Typhoon Saomai from the Joint Typhoon Warning Center (JTWC) and the monthly mean aerosol optical depth (AOD) at 550 nm, with the average in August 2006 from the Spectral Radiation-Transport Model for Aerosol Species (SPRINTARS) (Takemura et al., 2000; Takemura et al., 2002; Takemura et al., 2005). The AOD was markedly high over mainland China and gradually decreased toward the sea. After the TC genesis, Saomai moved northwestward and made landfall in the Zhejiang
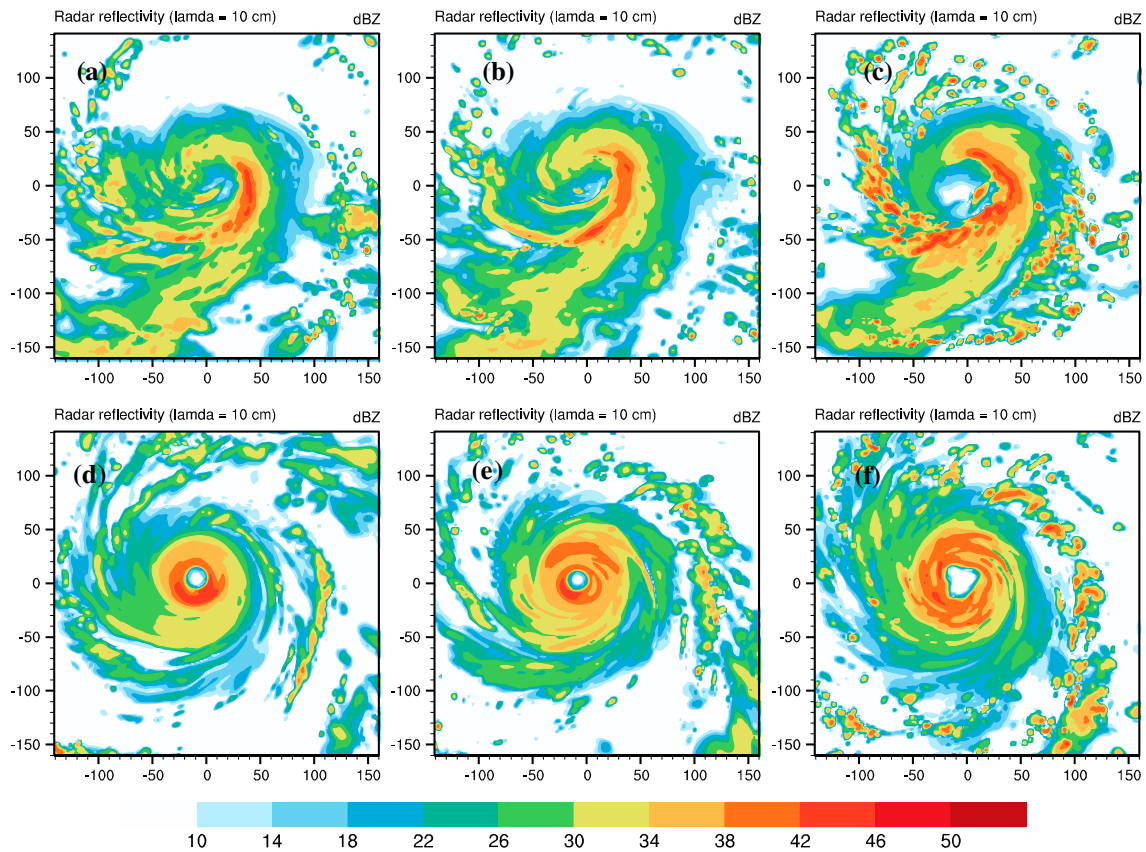
Figure 5. Fields of the radar reflectivity (dBZ) at 1 km at (top row) 0500 UTC on 8 August and (bottom row) 1000 UTC on 9 August for the (left column) MAR, (middle column) MIX, and (right column) CON simulations.

Province. The AOD pattern shown in Figure 1 provides the basis for designing the initial distribution of the aerosol in the semicontinental (MIX) simulation (see below).

To investigate the impacts of aerosol on the intensity, structure, and microphysical processes of Typhoon Saomai (2006), the WRF model (version 3.6.1) (Skamarock et al., 2008) with the SBM scheme was used; this spectral bin scheme is based on the SBM scheme included in the Hebrew University Cloud Model in Khain et al. (2004) and was described by Lynn and Khain (2007), Khain et al. (2009), and Khain (2009). The SBM scheme is based on the size distributions of seven classes of cloud hydrometeors: water drops, three types of crystals (columnar, plate-like, and dendrites types), aggregates (snow), graupel, and hail. Each spectrum is defined on a logarithmically equidistant doubling mass grid, which contains 33 mass bins, where the mass of the drop mass in the $(i + 1)$th bin is twice as large as that in the ith bin (Khain et al., 2009). The minimum mass in the hydrometeor mass grid (except CCN) corresponds to that of a 2 μm radius droplet, and the maximum bin of hydrometeors corresponds to the mass of a 4 mm radius drop. In contrast to the standard bulk parameterization schemes, the size distributions of the hydrometers and aerosol are not prescribed a priori but are calculated during the model integration. To increase the efficiency of the calculations, Lynn et al. (2005a, 2005b) proposed the first fast version of the SBM scheme (FAST-SBM). The FAST-SBM retains the main advantages of the SBM, in that a kinetic equation system is solved using the nonparameterized basic equations (Khain et al., 2009). However, in the FAST-SBM, the ice crystals (of different types) and snow (aggregates) are calculated on one mass grid, where the smallest ice particles, with sizes under 150 μm, are regarded as small crystals, while larger particles are assumed to be snow (aggregates). Graupel and hail particles are also combined into one size distribution (graupel) as high-density particles. The maximum velocity of the falling high-density particles is 8 m s^{-1} (33 bin), i.e., the intermediate value between graupel and hail. Accordingly, the number of size bins decreases from eight to four, including water drops (cloud droplets and raindrops), low-density ice (ice crystals and snow), high-density ice (graupel and hail), and CCN. The ability of the WRF with FAST-SBM to simulate squall lines, TCs, deep convective clouds, and
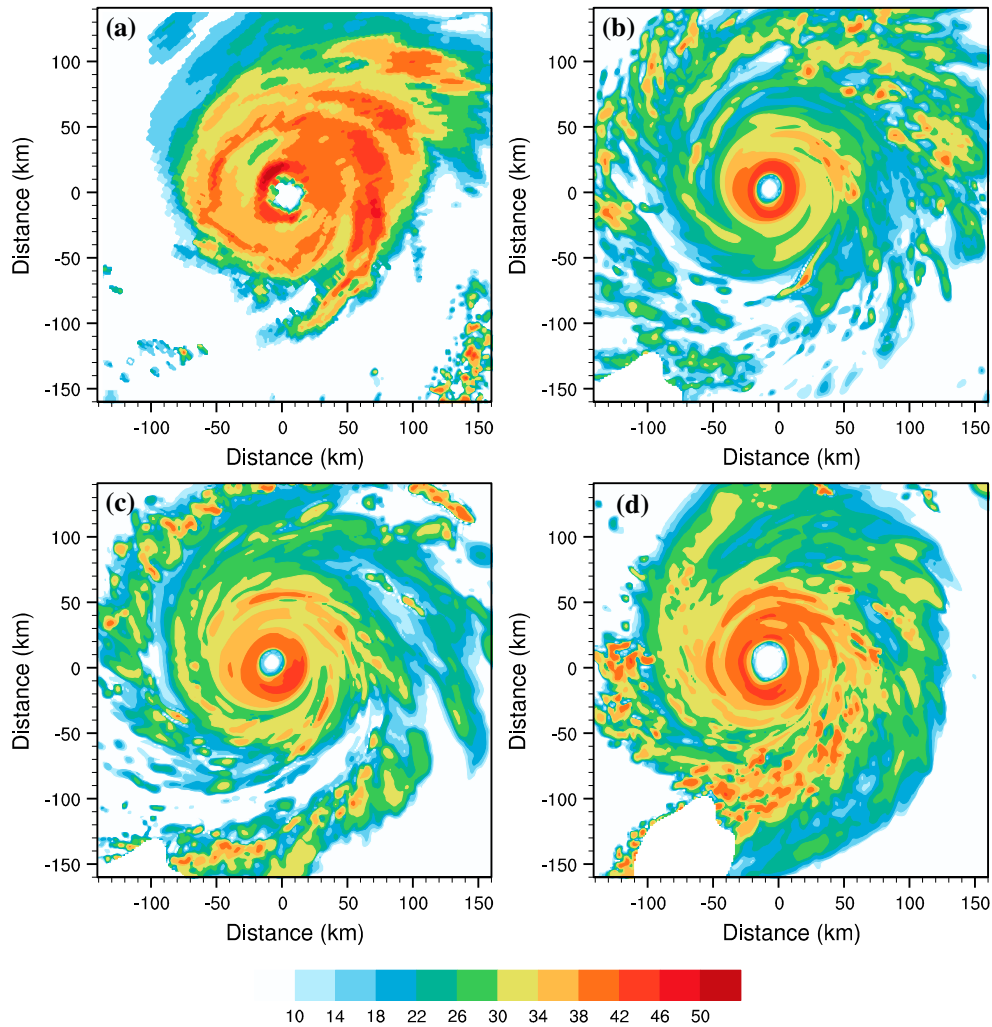
Figure 6. Fields of the radar reflectivity (dBZ) at 2000 UTC on 9 August at 1 km: (a) observational and (b) MAR, (c) MIX and (d) CON simulations.

stratiform clouds has been shown in the literature (e.g., Fan et al., 2012; Khain et al., 2009, 2010, 2016; Lynn & Khain, 2007; Lynn et al., 2016).

Two-way interactive nested grids with horizontal grid sizes of 12, 4, and 1.33 km were used, as shown in Figure 2. The horizontal grid points for the outer, intermediate, and inner domains were 240 × 180, 181 × 181, and 241 × 241, and the corresponding time steps were 20, 6.67, and 2.23 s, respectively. The intermediate and inner grids were structured as automatic vortex-following moving nests: the minimum geopotential height at 500 hPa was found every 20 min to ensure that the center of the domain was always located at the TC center. Forty unevenly spaced vertical levels extending from the surface to 10 hPa were used, with a minimum grid size of approximately 60 m within the boundary layer. The initial and boundary conditions were taken from the 6-hourly National Centers for Environmental Prediction (NCEP) final analysis (FNL) data sets, available at 1° × 1° resolutions. The simulations began at 1200 UTC on 7 August, 1800 UTC on 7 August, and 0000 UTC on 8 August 2006 for the outer, intermediate, and inner domains, respectively. All simulations ended at 0000 UTC on 11 August 2006.

The physical schemes adopted for this study include the Yonsei University planetary boundary layer scheme, Dudhia shortwave scheme, and Rapid Radiative Transfer Model longwave radiation schemes. The model used the Kain-Fritsch cumulus parameterization (Kain, 1993) on the outer grid, and the FAST-SBM scheme was used on all three domains.

The CCN size distribution contains 33 bins, and the maximum radius of CCN is equal to 2 μm. The CCN field can be advected within the entire computational area, such as other cloud hydrometeors. Supersaturation
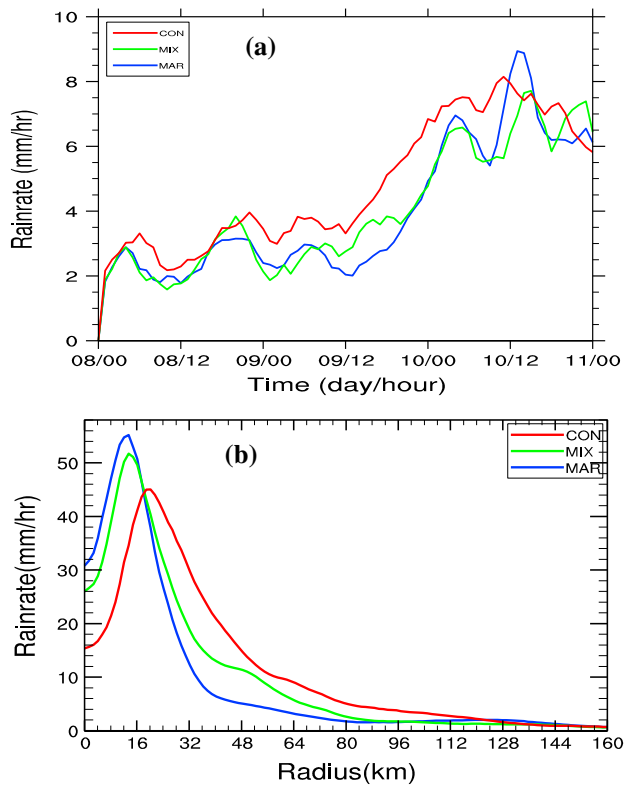
Figure 7. (a) Average precipitation rate (mm h^{-1}) for the three experiments averaged over an area of 320 km by 320 km for the 73 h in domain D3. (b) Azimuthally averaged and time-averaged precipitation rates (mm h^{-1}) from 1200 UTC on 9 August to 0000 UTC on 10 August in the MAR (blue line), MIX (green line), and CON (red line) simulations.

was calculated using an accurate analytical method at each time step, and the critical CCN size for drop activation was also calculated. No aerosols were returned to the atmosphere in case of evaporation (cloud/raindrop). The concentration of CCN, N_{CCN}, can often be expressed by an empirical relation of the form (Pruppacher & Klett, 1997)

$$N_{CCN} = N_o S_w k,$$

where S_w is the supersaturation with respect to water (%) and N_o and k are the constant parameters describing the CCN concentrations at a supersaturation level of 1% and the slope of the CCN size distribution, respectively.

Three sensitivity experiments were carried out to investigate the aerosol effects on the simulated Saomai and are referred to as the MAR, CON, and MIX experiments. The experiments only differed in the concentrations of CCN to investigate the effects of CCN on the structure and intensity of TCs. These experiments correspond to clean maritime, polluted continental, and mixed-continental aerosol conditions, respectively. The MAR simulation had only maritime aerosol over the entire computational domain, with $N_o = 100$ cm^{-3} and $k = 0.4$. The polluted continental aerosols were specified as $N_o = 4,000$ cm^{-3} and $k = 0.9$ over the entire domain. In the mixed-continental case, the ideal horizontal distribution of the CCN concentration was constructed based on the SPRINTARS data. There were polluted continental aerosol over the mainland, with $N_o = 4,000$ cm^{-3} and $k = 0.9$, and maritime aerosol over the sea, with $N_o = 100$ cm^{-3} and $k = 0.4$. Between the mainland and the open sea were two transition areas where N_o was set to 2,000 and 800 cm^{-3}, respectively (the shading in Figure 2 represents the CCN concentra-

tions in the MIX simulation). The MIX simulation was aimed at investigating the effects of the nonuniform horizontal aerosol distribution, caused by aerosol being transported from mainland China to the sea. The initial vertical CCN concentration distribution was assumed to be constant within the lowest 2 km layer but to decrease exponentially with height above 2 km, with a characteristic scale of 2 km.

3. Results and Discussions

3.1. Effect of Aerosol on the Intensity and Track of Saomai

Figure 3a compares the simulated tracks from three experiments with different aerosol concentrations and the best track from the JTWC at 6 h intervals. The simulated tracks were created from the data in domain
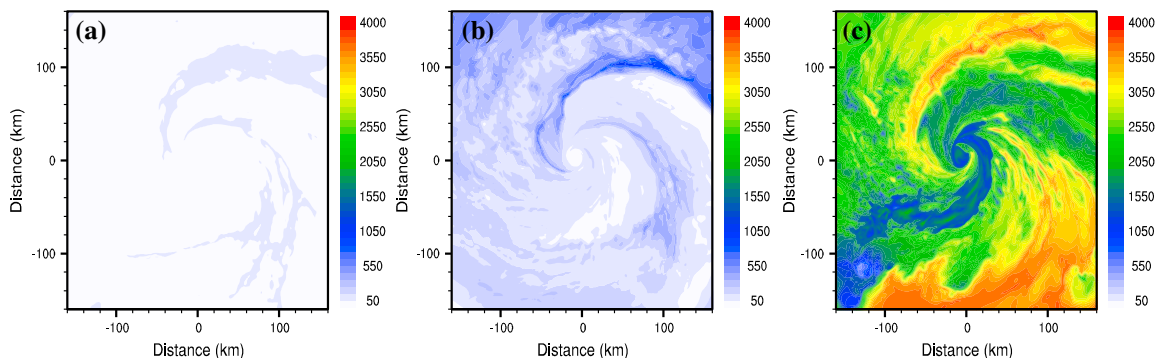

Figure 8. Horizontal fields of the column-maximum concentrations of aerosol in the domain D3 at 1700 UTC on 9 August (units: cm^{-3}) in the (a) MAR, (b) MIX, and (c) CON simulations.
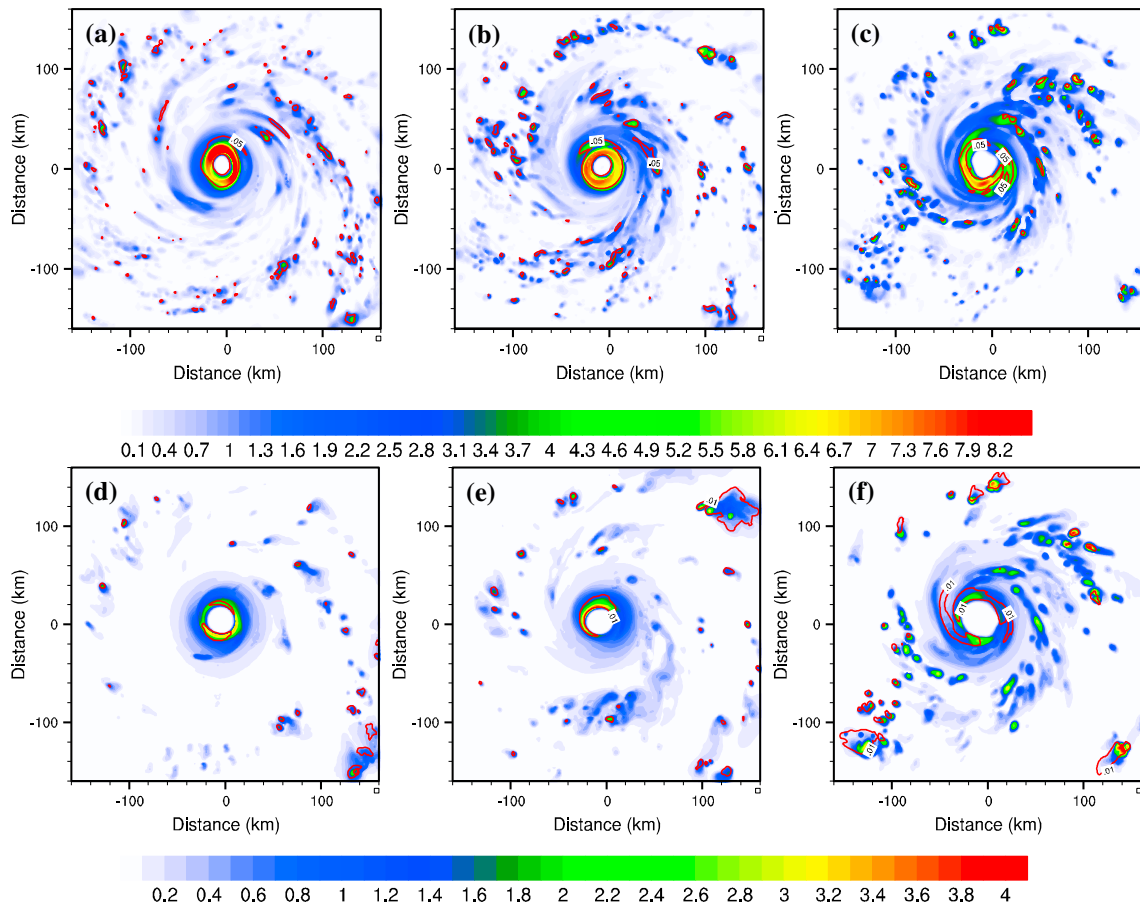
Figure 9. Horizontal fields of the column-maximum mass concentrations (colored) in g m^{-3} and with the maximum number concentrations (in units of cm^{-3}) of (top row) rainwater (contour, 0.05) and (bottom row) graupel (contour, 0.01) at 1700 UTC on 9 August on the fine grid in the (left column) MAR, (middle column) MIX, and (right column) CON simulations.

D1. Three simulated tracks agreed well with the observed track for the first 48 h. Each simulated TC moved northwest, but the simulations were slightly southwestward of the best track. Furthermore, the landfall locations of three simulated TCs all occurred slightly southward. The track errors from 1200 UTC on 7 August to 0000 UTC on 11 August are shown in Figure 3b. The MIX and MAR simulations had slightly less track errors than the CON simulation. Figure 3c depicts the tropospheric-averaged steering flows, averaged from 0600 to 1200 UTC on 9 August and from 0600 to 1200 UTC on 10 August in the D3 domain, as well as the difference vectors. The tropospheric-averaged steering flow in the deep-layer mean wind vector was defined as in Yang and Ching (2005):

$$V_{\text{SDLM}} = \frac{\int_{ps}^{200 \text{ hPa}} V_S(p)dp}{\int_{ps}^{200 \text{ hPa}} dp},$$

where $V_S(p)$ is the horizontal wind averaged over the fine grid (320 km by 320 km). It is noted that the steering flows mainly determine the simulated TC tracks. The CON (MAR) run had the most (least) westward steering flow and thus the most (least) westward simulated track. There occurred Typhoon Bopha (2006) in the southern of Typhoon Saomai. The small differences between three TC tracks were possibly due to the strong environmental control of the track of Typhoon Bopha (2006).

Figure 4 shows the time evolution of the minimum central pressure (Figure 4a) and 10 m maximum wind speed (Figure 4b) in domain D3 from three experiments and the observations in the JTWC data set. After the model spun up for 12 h in the outer two grids, the simulated TC had a lower intensity during the first 36 h in domain D3 compared to that of the actual Saomai. Furthermore, the model was capable of reproducing the TC intensification. As shown in Figure 4, TC intensified in CON simulation during the first 18 h. After
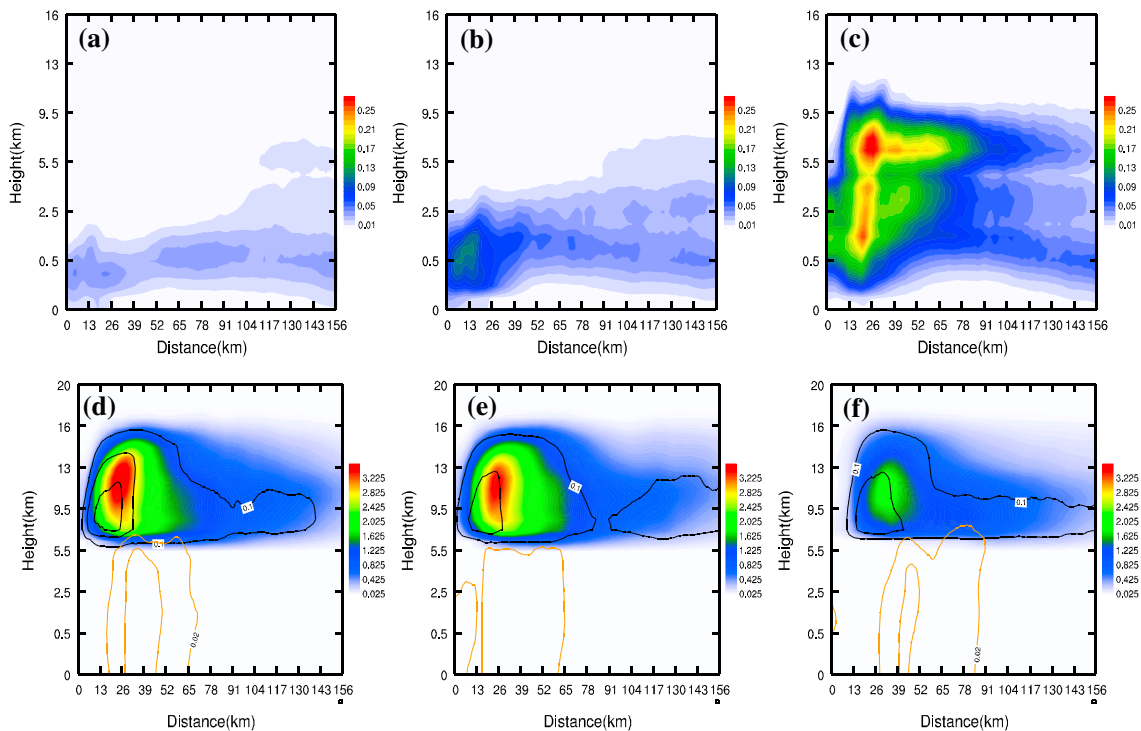
Figure 10. The vertical cross section of the azimuthally averaged (top row) mass concentrations of cloud water, (bottom row) mixing ratios of graupel (black line, at 0.01, 0.1, 0.5, and 1), rainwater (orange line, in 0.02 and 0.05), and ice/aggregates (colored) in units of g kg^{-1}, averaged over 0600 UTC on 9 August and 1800 UTC on 10 August in the (left column) MAR, (middle column) MIX, and (right column) CON simulations.

1800 UTC on 8 August MAR simulation produced stronger TC than the other two. Similar results have also been reported in previous simulations (e.g., Krall & Cottom, 2012; Rosenfeld et al., 2012). The explanation of these results was about the time when CCNs were intruded into the eyewall and rainbands (shown below in section 3.2). When the TC reached its maximum intensity, the minimum surface pressure (maximum wind speeds) of the CON and MIX simulations were approximately 30 hPa (20 m s^{-1}) and 14.6 hPa (13 m s^{-1}) weaker than that in the MAR simulation, respectively. Furthermore, the typhoon intensity was found to be sensitive to the aerosol concentration. The mechanisms of aerosol effects weakening TCs were discussed in detail by Rosenfeld et al. (2012).

3.2. Effect of Aerosol on the Structure of Saomai

The fields of the radar reflectivity at 1 km at 0500 UTC on 8 August and 1000 UTC on 9 August are shown in Figure 5. Before 1800 UTC on 8 August, the CON simulation produced a stronger TC than the other two because the increased aerosol in this experiment invigorated the convections in the eyewall. The dramatic intensification of convection caused by aerosol can be clearly observed in Figure 5c. For example, at 0500 UTC on 8 August (Figures 5a–5c), the MIX and MAR simulations had similar reflectivities because the aerosol particles had not been ingested into their circulations at the beginning (both storms developed in relatively pristine environments). As a result of aerosol effects in CON, a pronounced eye was formed. Later on aerosol was not only intruded into the eyewall but also into the rainbands. At 1000 UTC on 9 August, the CON and MIX simulations had stronger reflectivities in their peripheries than the MAR simulation (shown in Figures 5d–5f). Strong rainbands formed in the MIX and CON experiments, particularly for the CON simulation. The stronger convections in the eyewall and rainbands competed with each other; that is, the vertical updrafts in these two areas were competitive. The convective updrafts in eyewall were weakened, leading to weaker typhoon after 1800 UTC on 8 August.

The inner rainbands occurred in the inner-core region, inside a radius of approximately 3 times the radius of the maximum wind (RWM), as defined by Wang (2009). The outer rainbands were active outside 3 times the RWM (Li & Wang, 2012). The RMWs in the MAR, MIX, and CON simulations were 12 km, 15 km, and 20 km, respectively. In this paper, the area within the inner rainbands represents the region from eye area to the

inner rainbands. At the developing stage (from 1800 UTC on 8 August to 1200 UTC on 9 August) and mature stage (from 1200 UTC on 9 August to 0000 UTC on 10 August), the invigorated convection in the outer rainbands competed with those within the inner rainbands, leading to a weaker typhoon in the MIX and CON experiments than that in the MAR experiment. This weakening can be seen in the increase of the radius of the eyewall in the CON run. The "convection-competition" effect ultimately led to a weaker TC in the MIX and CON runs, which agreed with the conceptual model proposed by Khain et al. (2009); specifically, an increase in the vertical velocity (updraft) at the TC periphery produced a competition for environmental moisture between the TC eyewall and the periphery, leading to a suppressed TC.

Figure 6 shows the comparison of the simulated and observed radar reflectivities at 1 km at 2000 UTC on 9 August. Overall, the three simulations showed weaker reflectivities than those observed, especially over the outer rainbands. Moreover, their comparison indicates that the MIX run simulated better radar echoes in the eyewall and secondary eyewall than the other two runs. Moreover, the evolution of the simulated storm intensity in the MIX run was the closest to that observed (shown in Figure 4). Note that the eye in the CON experiment was wider than those in the other two simulations, causing the weakest intensity at the mature stage. The simulated TC eye area with the FAST-SBM scheme in this study was smaller and closer to the observed than that simulated using bulk microphysics schemes (Ming et al., 2012). Therefore, the FAST-SBM scheme is better at simulating the structure of Saomai than the bulk microphysical schemes to an extent. The strong intensity of simulated TC could be attributed to the fact that the sea surface temperature (SST) cooling below the TC center was not considered by our calculations.

3.3. Precipitation

Figure 7a shows the precipitation rate for the three experiments, which is averaged over the area of 320 km by 320 km from 0000 UTC on 8 August to 0000 UTC on 11 August. Three simulations showed similar rain rates over the first several hours. However, the rain rate in CON simulation clearly increased (compared with those of the other two simulations) in the following hours, especially during the developing and mature stages. The rain rate in the CON simulation was 16.6% and 56.2% higher than those in the MIX and MAR experiments, respectively. Figure 7b compares the radial distribution of the azimuthally averaged rain rate, which was averaged from 1200 UTC on 9 August to 0000 UTC on 10 August. The simulations (MIX and CON) with higher CCN concentrations had wider eyewalls, and lower rain rates in the eyewalls, but in outer rainbands, they had higher rain rates than that of the MAR simulation.

The cloud microphysics precipitation efficiencies (CMPE) defined by Sui et al. (2007) in domain D3 were 54.15%, 54.55%, and 54.77% for the MAR, MIX, and CON simulations, respectively. The CMPE did not change significantly with different CCN concentrations, although the CMPE in the CON simulation is slightly higher than those in the other two simulations. The MIX simulation was found to have a higher CMPE within the inner rainbands than the other two simulations. This CMPE tendency within the inner rainbands agreed well with the tendency of rain rate there (not shown). However, in the outer rainbands, more aerosols led to higher rain rates and lower CMPEs because much more water vapor condensed to cloud droplets with higher CCN concentrations. The two main sources of rainwater were graupel melting and the collection of cloud droplets by raindrops. More details of the microphysical comparisons will be discussed in section 3.5.

3.4. Distribution of Aerosol

To better understand the effects of aerosol on Saomai, we focus on the period from 1200 UTC on 9 August to 0000 UTC on 10 August. During this period, Saomai was affected by continental aerosol while approaching the mainland (Figure 1). Figure 8 shows the fields of the column-maximum number concentration of aerosol in the D3 domain at 1700 UTC on 9 August. The aerosol concentrations of the CON experiment were always higher than those in other two simulations; all three simulations had a new portion of CCN being activated and producing droplets when the typhoon approached the mainland. The aerosol concentration decreased when approaching the TC center, as a result of aerosol activation (acting as CCN) through nucleation scavenging of cloud droplets, similar to the results in Khain et al. (2010).

3.5. Effects of Aerosol on the Cloud Microphysics of Saomai

Figures 9a–9c show the fields of the column-maximum mass concentration and number concentration of rainwater in domain D3 in the three simulations at 1700 UTC on 9 August. Note that there were more

raindrops within the inner rainbands of the MAR and MIX simulations. The larger amount of CCN in the CON simulation led to a corresponding decrease in cloud droplet size, which decreased the autoconversion rate of the cloud droplets to raindrops. Thus, the number concentration of raindrops decreased in the experiment with higher CCN concentrations. The CON simulation had broader rainbands and a larger eye than the other two experiments. The CON simulation had a higher rainwater mixing ratio in its outer rainbands, but the number concentration of raindrops was lower; thus, the raindrops were larger (not shown). More cloud water could be collected by the raindrops, leading to larger raindrops. The aerosol-induced changes in the warm rain microphysics resulted in corresponding changes in the ice microphysics (Khain et al., 2009). Figures 9d–9f show the column-maximum mass and number concentration of graupel at 1700 UTC on 9 August. With higher CCNs, there was a higher graupel content in the outer rainbands and a lower one within the inner rainbands. The larger graupel particles in the CON simulation resulted in more graupel melting, which could explain the similar horizontal distribution of rainwater and graupel. The MIX and CON simulations had more ice-phase contents in their outer rainbands, indicating more efficient mixed-phase processes to produce rainwater (Figures 9a–9c).

To better understand the vertical distribution of the various hydrometeors, Figure 10 presents a vertical cross section of the azimuthally averaged contents of each hydrometeor in domain D3, averaged from 1200 UTC on 9 August to 0000 UTC on 10 August. The maximum heights of cloud water in three simulations (shown in Figures 10a–10c) are distinctly different. In the MAR and MIX simulations, the cloud water could reach heights of 5 km. However, cloud droplets could rise above 10 km in the CON simulation, especially within the inner rainbands, producing more supercooled cloud droplets. The CON simulation clearly had more liquid water content and was wider in the radial direction. An increased number of smaller-sized cloud droplets were easily transported upward by strong updrafts. In the FAST-SBM scheme, the ice crystals and snow (aggregates) are calculated in one mass grid. The MIX simulation had a higher content of aggregates than the other two experiments. The consistent increase of the aggregate content continued until the CCN reached higher values, after which a "tipping-point" was verified that prevents further increases in CCN concentrations leading to a greater production of aggregates (shaded in Figures 10d–10f). More droplets in the MIX and CON simulations grew via vapor diffusion, ascending with more efficient freezing. The sources of the cloud ice include deposition growth, homogeneous freezing of cloud water, and the freezing process. However, the amount of cloud ice was much smaller than that of snow. Thus, snow accounted for the vast proportion of aggregates. The snow was mainly generated from deposition growth and riming process, and the decreased deposition growth in the CON simulation led to fewer aggregates. As shown in Figures 10d–10f, for higher CCNs, the horizontal distribution of graupel extended further from the TC center, similar to the results of Lynn et al. (2016). The major source of graupel in the outer rainbands was the liquid riming to graupel. With higher CCN concentrations (MIX and CON simulation), the rainwater mixing ratio within the inner rainbands was decreased, which agreed with the horizontal distribution results (Figures 9a–9c). However, the rainwater mixing ratios of the outer rainbands were increased, and the raindrops could reach higher heights than those in the MAR simulation. Thus, with higher CCNs, the enhanced precipitation processes in the outer rainbands led to more TC rainfall.

3.6. Effects of Aerosol on the Microphysical Conversion Processes

Quantifying the conversion processes between all types of hydrometeors is important to understand the cloud microphysics and precipitation processes. More details of the mass contents of the hydrometeors and the production rate of the major microphysical processes averaged across different areas (within the inner rainbands, in the outer rainbands, and the whole D3 domain) are shown in Figures 11–13. The units of the hydrometeor contents and conversion rates are kg m^{-2} and kg m^{-2} h^{-1}, respectively. If the contents of the hydrometeors and their production rates increased (decreased) with higher amounts of CCN concentrations, they were denoted in red (blue).

Figure 11 shows the diagram of each hydrometeor and its corresponding production rate of microphysical processes in the FAST-SBM scheme, averaged from 1200 UTC on 9 August to 0000 UTC on 10 August within the inner rainbands. The symbol definitions are shown in Table 1. With higher CCNs, the cloud water and cloud ice contents and their major generation processes increased; on the other hand, the contents of other hydrometers (rainwater, snow, and graupel) and their production processes were all suppressed. This indicates that aerosol-induced precipitation processes were suppressed within the
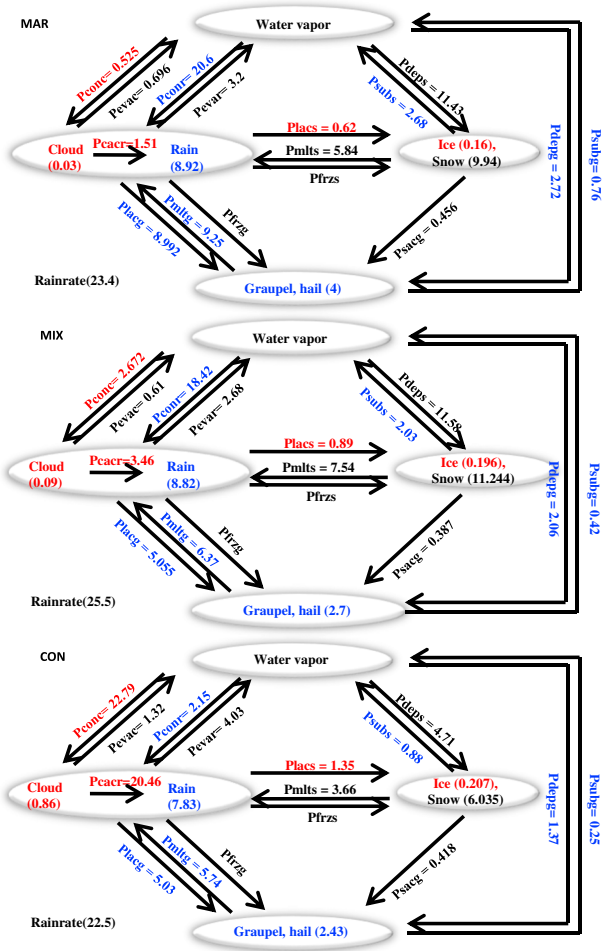
Figure 11. Diagram of each hydrometeor and the corresponding rate of change of the microphysical process in the FAST-SBM scheme, averaged from 1200 UTC on 9 August to 0000 UTC on 10 August in the inner rainbands. The meanings of the acronyms are shown in Table 1; the values are vertical integration of each variable, and the units of the hydrometeors and the rates of change are in kg m^{-2} and kg m^{-2} h^{-1}, respectively, and the values of the rates of change increased (decreased) when more aerosols are donated in red (blue).

inner rainbands. Figure 12 shows the same information except for the average in the outer rainbands. Note that the averaged values within the inner rainbands (Figure 11) were larger than those in the outer rainbands (Figure 12) because the area of inner rainbands was small and the hydrometeors were mainly concentrated in this area. In the outer rainbands, most of the microphysical processes were invigorated by additional CCNs. Cloud water and cloud ice were also increased in the CON outer rainbands. However, the trends of the rainwater and graupel contents were different from those within the inner rainbands, mainly because more riming occurred and led to more graupels. Thus, these more graupels would melt to more rainwaters, and more collections of cloud water by additional rainwater were found, leading to more precipitations in the CON outer rainbands. That is, there was a positive microphysics feedback in the outer rainbands. The rainwater contents in the MIX and CON simulations were 12% and 21.7% larger than that in the MAR simulation, respectively. With higher CCN concentrations within the inner rainbands, there were decreasing growth rates of the deposition and riming processes. In the outer rainbands, more graupels were found; graupel contents in the MIX and CON simulations were 32% and 78.6% larger than that in the MAR experiment, because the locally riming processes in the MIX and CON experiments were 1.5 and 3 times that in the MAR experiment, respectively.

Figure 13 presents the averaged values for the domain D3. Most hydrometeors increased with higher CCNs in domain D3, except for those aggregates that had a "tipping-point" (i.e., the MIX run had the highest snow content). This indicates that most of the microphysical processes were reinforced. The cloud water content in the CON run was approximately 4 times larger than that in the MAR run, mainly because of the increased water vapor condensing to cloud droplets. Although there was more liquid water rimed to aggregates in the CON simulation, the mass produced from that riming was approximately 10 times less than that from deposition growth (shown in Figure 13). The riming process coupled the deposition growth to form aggregates, leading to the "tipping-points" in aggregates. In the outer rainbands, the riming process played a dominant role in graupel formation. The melting rate of the graupel in the CON simulation was 2.7 and 1.3 times larger than those in the MAR and MIX simulations, respectively, and was mainly concentrated in the outer rainbands. In the CON simulation, the distribution of the larger graupel particles was relatively sparse, and the larger graupel particles were found mostly in the outer rainbands (not shown), leading to higher mass concentrations of graupel there. Although the graupel amounts in the outer rainbands were smaller, overall, the outer rainbands agreed well with those averaged in the whole domain D3 (the colors in Figures 12 and 13 are similar).

4. Summary and Conclusions

In this study, the effects of aerosol on Typhoon Saomai (2006) were studied using the fast version of the explicit spectral bin microphysics (FAST-SBM) scheme implemented with the Weather Research and Forecasting (WRF) model over a 1.33 km horizontal grid spacing. For the first time, the FAST-SBM scheme was utilized to quantify the microphysical processes for varying amounts of aerosol in a typhoon over the Western Pacific. The evolution of Typhoon Saomai was simulated from 1200 UTC on 7 August to 0000 UTC on 11 August 2006. Three sensitivity experiments were conducted to examine the indirect effects of the aerosol on the structure, intensity, track, and precipitation of Saomai, namely, the MAR (N_o was set equal to 100 cm^{-3}), MIX (N_o was set to have gradients of 4,000; 2,000; 800; and 100 cm^{-3}, respectively), and CON (N_o was set equal to 4,000 cm^{-3}) experiments. The initial aerosol distributions over the inner grid could be
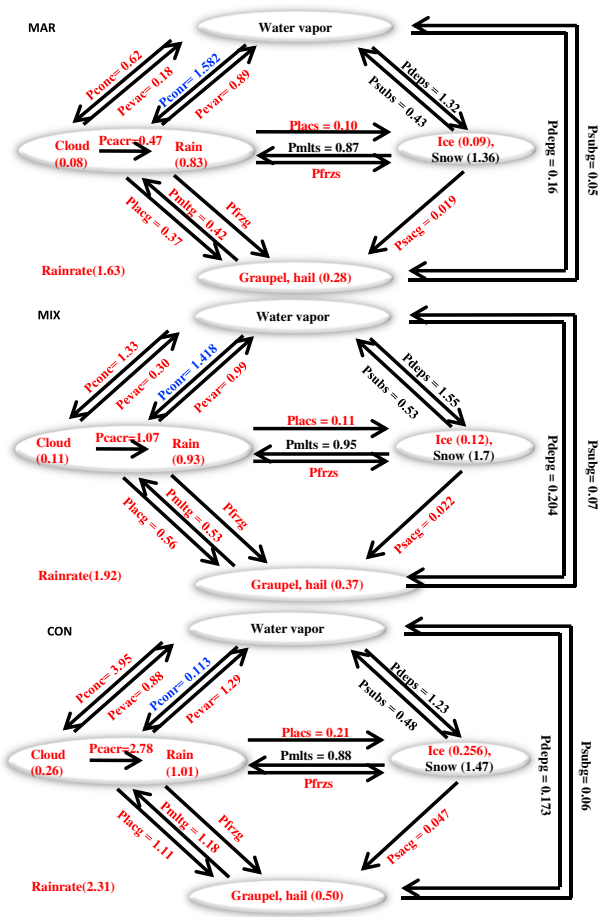
Figure 12. Same as in Figure 11 except for those averaged in the outer rainbands.

entrained into the TC circulation and serve as cloud condensation nuclei (CCN), influencing the microphysical processes and precipitation. The main conclusions are summarized as follows:

1. The intensity of the typhoon was sensitive to the CCN concentration. Before 1800 UTC on 8 August, the CON simulation had the strongest TC of the three experiments. Then, from 1800 UTC on 8 August to 1200 UTC on 9 August, more CCNs added to the CON and MIX simulations ultimately weakened the TC via the "convection-competition" effect between the eyewall and rainbands. The minimum sea level pressures were increased by 30 hPa and 15 hPa in the CON and MIX simulations, and the maximum surface wind speeds were weakened by approximately 20 m s^{-1} and 13 m s^{-1}, respectively. The three experiments had similar TC tracks due to the strong control of the environmental flows, although the CON (MAR) run simulated the most (least) westward track because the CON (MAR) run had the most (least) westward steering flow.

2. The CCN concentrations affected the structure and precipitation of the TC. The CON simulation had a stronger convection in its eyewall than the other two experiments during the beginning period. However, in the developing and mature stages, the "convection-competition" effect ultimately led to weaker TCs in the MIX and CON runs. Moreover, the MIX run was the most realistic simulation in terms of TC intensity and structure. Thus, including the observed aerosol concentrations may improve TC simulations. Many more TC cases remain to be tested in the future. The rain rate in the CON simulation was 16.6% and 56.2% higher than those in the MIX and MAR runs, respectively. The precipitation efficiency in the CON run was slightly larger than those in the other two, which agrees with their rain rates. The main microphysical processes producing raindrops in the outer rainbands were graupel melting and the accretion of cloud droplets by raindrops.

3. With high CCNs, the most obvious microphysical feature was the increase of the cloud water mixing ratio. An increased number of smaller-sized cloud droplets had lower efficiency in collisions and coalescences, leading to fewer raindrops within the inner rainbands. However, in the outer rainbands, more raindrops and graupel particles were found. The enhanced riming process in the outer rainbands led to an increase in the amount of larger-sized graupel particles. In addition, the efficient riming conversion of liquid droplets to graupel in the outer rainbands played a crucial role in graupel formation. Aggregates had two main formation processes: depositional and riming growth, the combination of which led to a "tipping-point" in the aggregate content when more CCNs were added.

4. A conceptual model of the distribution of the cloud hydrometeors and airflow in the inner and outer rainbands of a TC over maritime and continental environments, which is based on the above three sensitivity experiments, is shown in Figure 14. Convection in outer rainbands was enhanced by increased CCN contents. "Convection-competition" is the effect leading to weaker convection in inner rainbands, and the boundary layer inflow into the inner rainbands is partially blocked. In the continental environment, the melting level was raised and the rainbands spread wider; within the inner rainbands, there were smaller cloud droplets, smaller aggregates, fewer raindrops, and fewer graupel particles; in the outer rainbands, increased numbers of large graupel particles were found, some of which could melt into larger raindrops. These larger raindrops could collect more cloud droplets, leading to more rainfalls over the outer rainbands. On the one hand, the paper resulted similar conclusions with those of previous studies; e.g., the increase in CCN concentrations could intensify the convections in the outer rainbands but suppress the eyewall development, leading to weaker TCs ultimately. On the other hand, the microphysical processes were quantitative analysis, which also explained higher rain rate in CON simulation. Higher rain rates in the CON simulation are attributed to the enhanced coalescence and melting processes.
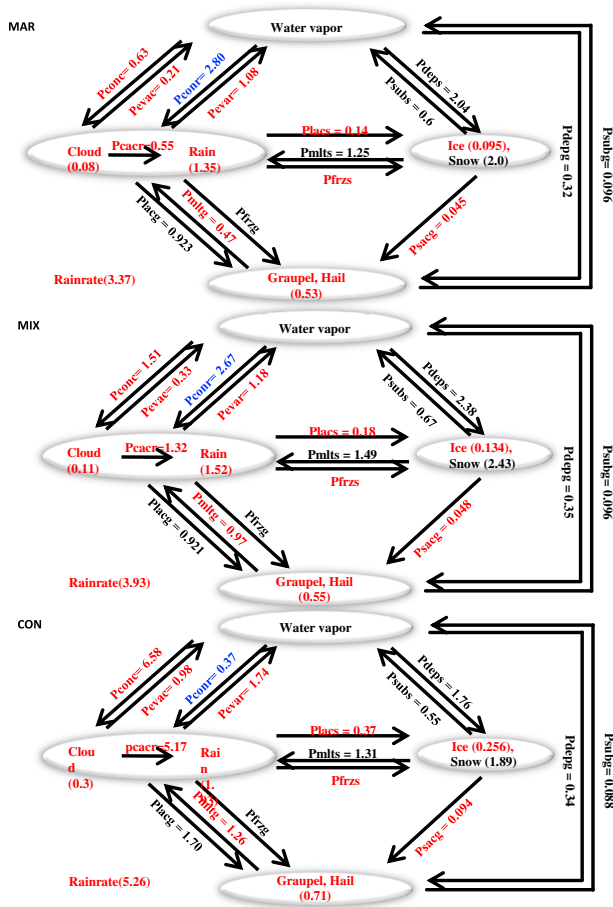
Figure 13. Same as in Figure 11 except for those averaged in the whole domain D3.

More CCNs can lead to more condensation and thereby release more latent heat. And the effects of CCN on the rainfall difference between different CCN scenarios mainly concentrated in the outer ranbands. In addition, the melting level in this study is higher than those in previous hurricane simulations. The simulated environment in this typhoon case study is warmer and moister than that in other hurricane cases. This may be due to the different environmental conditions between the previously studied TCs and current typhoon. For example, Ming et al. (2015) used dropsonde data from several typhoon and hurricane cases and found that typhoons are moister at lower levels than hurricanes, especially in their outer regions.

5. The processes of cloud condensation/evaporation, the autoconversion of the cloud water, and the collection of the cloud droplets by raindrops, liquid water riming, graupel melting, and rain rates were all increased in the D3 domain as the number concentration of CCN increased. In general, CCN affected the microphysical structure of the TC mainly through its effects on the outer rainbands. More graupels were shown in the outer rainbands, leading to more graupel melting, larger raindrops, and an increased collection of cloud droplets by raindrops. Thus, a positive microphysics feedback of rainwater was shown in the outer rainbands. With higher CCN concentrations, the balance of the microphysics budget in the outer rainbands was similar to that across the entire D3 domain.

In summary, we conclude that aerosol acting as CCNs can significantly affect the microphysical processes of clouds and the intensity, structure, and precipitation distribution of Typhoon Saomai, even with minor effects on the storm track. Although conclusions drawn in this paper are based on a landfalling typhoon, another typhoon Talim (2005) has also been operated with sensitivity experiments under different aerosol concentration conditions applying the same approach with Typhoon Saomai, including the experiment design and physical schemes. Typhoon Talim (2005) was simulated under maritime and continental aerosol environment to compare the variability of microphysics. Figure 15 shows the hydrometeors and microphysical processes averaged within the inner rainbands, in the outer rianbands, and the whole domain D3 of Typhoon Talim (2005). The colors in the three regions were similar to those in Saomai, which represented the trends of microphysics with more aerosols. The consistent findings are achieved with those in Typhoon Saomai (2006), i.e., CON simulated weaker

Table 1
Meaning of Each Symbol in Figures 11–13 and 15

| Symbol	Meaning	Symbol	Meaning
Cloud	Content of cloud water	Pfrzs	Rain freezing to ice and snow
Rain	Content of rainwater	Pmltg	Graupel melting to rain
Snow	Content of snow	Pmlts	Ice and snow melting to rain
Ice	Content of cloud ice	Pconc	Condensation to cloud water
Graupel, hail	Content of graupel and hail	Pevac	Evaporation of cloud water
Rain rate	Precipitation rate	Pconr	Condensation to rainwater
Placr	Accretion of water by ice and snow	Pevar	Evaporation of rainwater
Placg	Accretion of water by graupel	Pdeps	Deposition to ice and snow
Psacg	Accretion of ice and snow by graupel	Psubs	Sublimation of ice and snow
Pcacr	Collection of cloud water by rain and autoconversion of cloud to rain	Pdepg	Deposition to graupel
Pfrzg	Rain freezing to graupel	Psubg	Sublimation of graupel
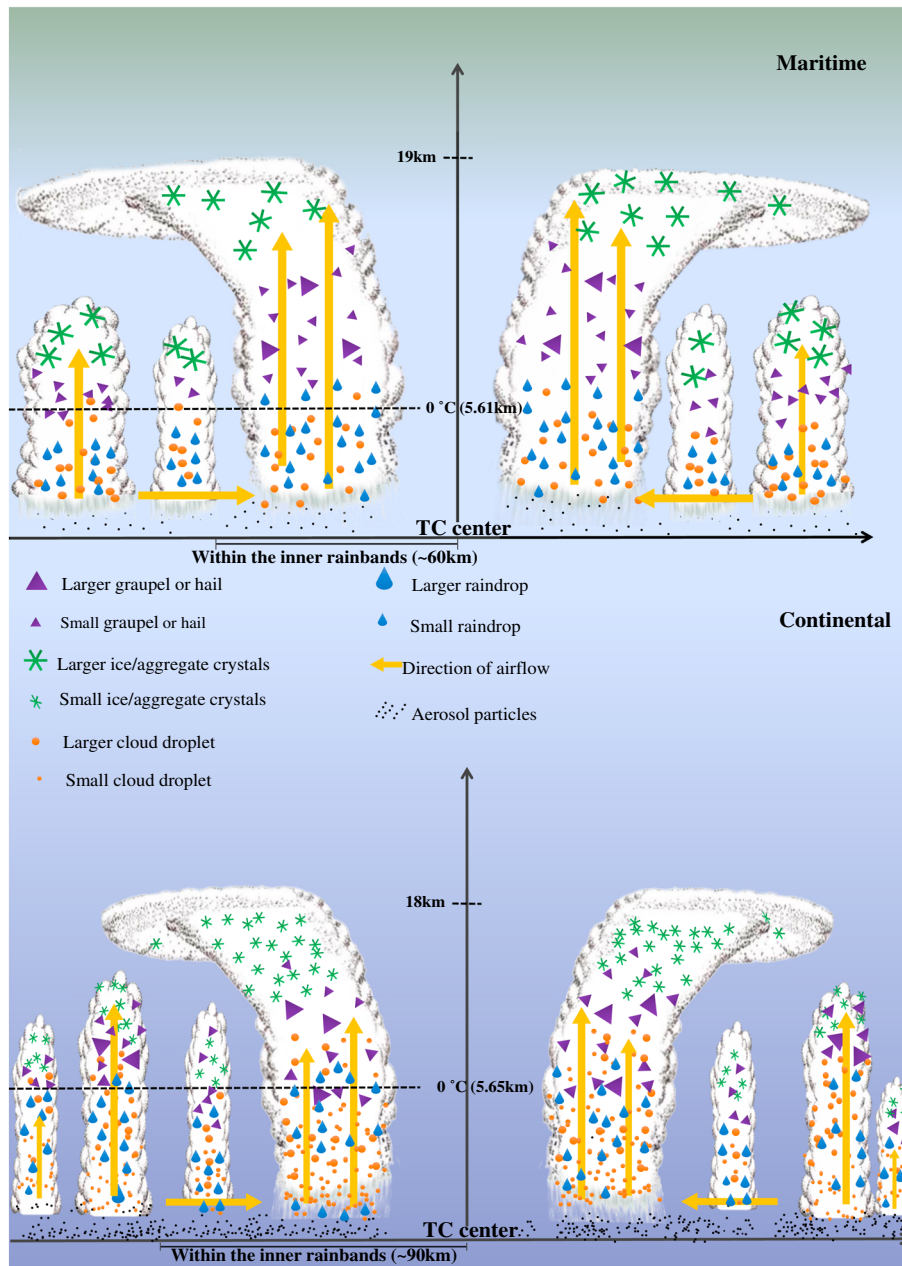
Figure 14. The conceptual model of the distribution of the cloud hydrometeors and airflows in the inner and outer rainbands of Typhoon Saomai (2006) for (top) maritime and (bottom) continental environments. The smaller cloud droplets have lower collision-coalescence efficiency, leading to fewer raindrops in the inner rainbands. Larger graupel or hail particles in the outer rainbands melt into larger raindrops in the outer rainbands. The convection of the outer rainbands in the continental environment was stronger, so the boundary layer inflow air in the inner rainbands was weaker.

typhoon than MAR simulation. The rain rate averaged within the inner rianbands was suppressed by more aerosols; however, precipitation was invigorated in the outer rainbands, so did it in the whole domain D3. There was more cloud water and ice in CON simulation. The riming processes were enhanced in the outer rainbands by more aerosols, which resulted in more graupels, more rainwaters, and higher rain rate in CON experiment.

Many issues will require further research. For example, the results about aerosol-induced effects on the dynamics and thermodynamics of typhoons need more explanations. Maybe future work based on the Saywer-Eliassen balanced equation will be helpful to explain the effects. Another one is the impact of aerosol acting as ice nuclei on TCs. Further simulations of the microphysics processes within the TCs are necessary to
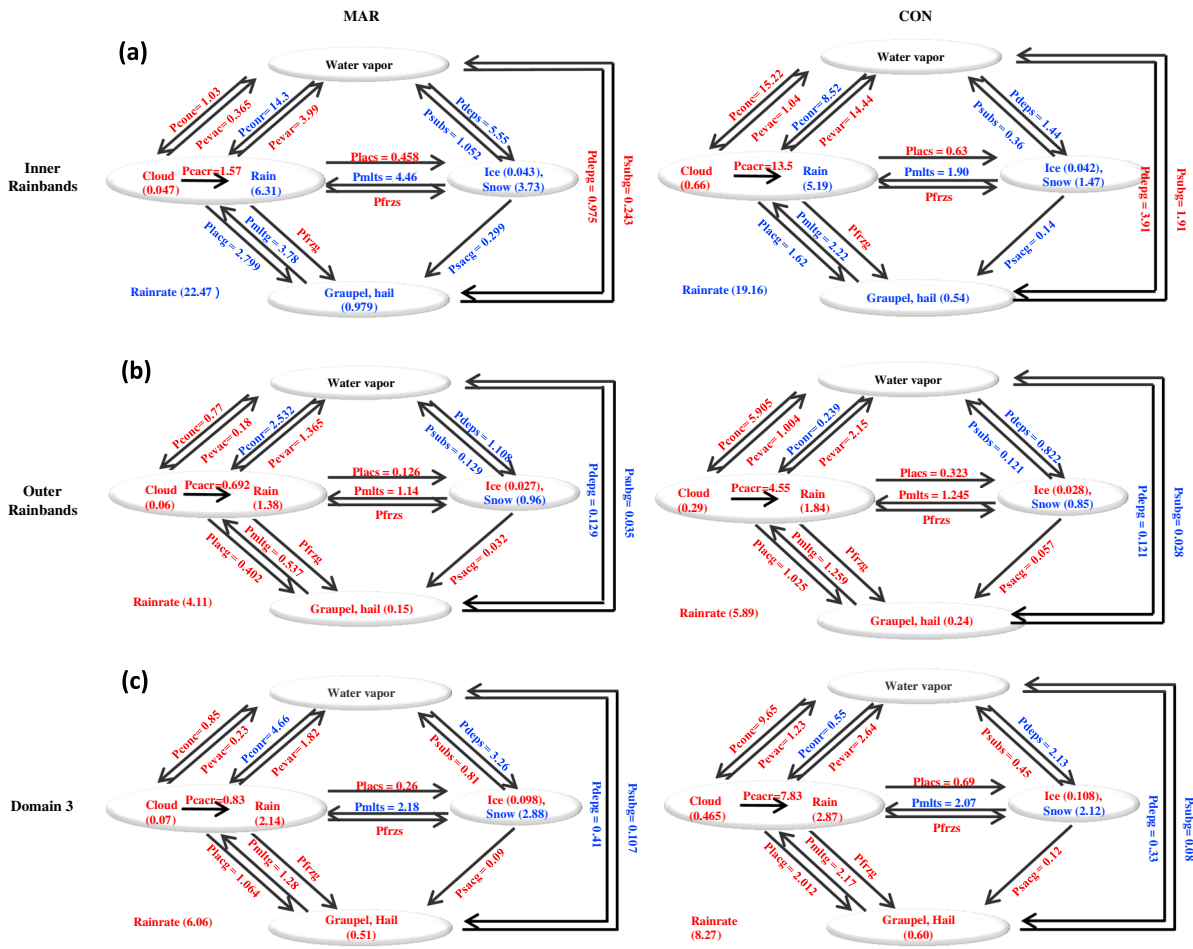
Figure 15. Diagram of each hydrometeor and the corresponding rate of change of the microphysical process in the FAST-SBM scheme, averaged from 0600 to 1200 UTC on 30 August (a) within the inner rainbands, (b) in the outer rainbands, and (c) in the whole D3 for (left) MAR and (right) CON simulations of Typhoon Talim (2005). The meanings of the acronyms are shown in Table 1; the values are vertical integration of each variable, and the units of the hydrometeors and the rates of change are in kg m^{-2} and kg m^{-2} h^{-1}, respectively, and the values of the rates of change increased (decreased) when more aerosols are donated in red (blue).

verify our modeling results based on a single TC case. Additionally, future work on this topic, such as quantifying the effects of sea-salt aerosol, which play an important role in the maritime environment as giant aerosol, is needed. TC Saomai (2006) is an axis-symmetric TC; thus, additional future research should investigate the indirect effects of CCNs on asymmetric TCs by more experiments in the future.

References

Anthes, R. A. (1982). *Tropical cyclones: Their evolution, Structure, and Effects, AMS Meteorology Monographs* (Vol. 41, 208 pp.). Boston, MA: American Meteorological Society. https://doi.org/10.1007/978-1-935704-28-7

Cotton, W. R., Zhang, H., McFarquhar, G. M., & Saleeby, S. M. (2007). Should we consider polluting hurricanes to reduce their intensity? *Journal of Weather Modification*, 39, 70–73.

DeMaria, M., Mainelli, M., Shay, L. K., Knaff, J. A., & Kaplan, J. (2005). Further improvements to the Statistical Hurricane Intensity Prediction Scheme (SHIPS). *Weather Forecasting*, 20(4), 531–543. https://doi.org/10.1175/WAF862.1

Duan, Y. H., Lianshou, C., Yinglong, X., & Chuanhai, Q. (2012). The status and suggestions of the improvement in the typhoon observation, forecasting and warning systems in China. *Engineering Sciences*, 9, 003.

Emanuel, K. (2005). *Divine wind: The history and science of hurricanes* (296 pp.). New York: Oxford University Press.

Evan, A. T., Kossin, J. P., Chung, C. E., & Ramanathan, V. (2011). Arabian sea tropical cyclones intensified by emissions of black carbon and other aerosols. *Nature*, 479(7371), 94–97. https://doi.org/10.1038/nature10552

Fan, J., Leung, L. R., Li, Z., Morrison, H., Chen, H., Zhou, Y., … Wang, Y. (2012). Aerosol impacts on clouds and precipitation in eastern China: Results from bin and bulk microphysics. *Journal of Geophysical Research*, 117, D00K36. https://doi.org/10.1029/2011JD016537

Fan, J., Leung, L. R., Rosenfeld, D., Chen, Q., Li, Z., Zhang, J., & Yan, H. (2013). Microphysical effects determine macrophysical response for aerosol impacts on deep convective clouds. *Proceedings of the National Academy of Sciences of the United States of America*, 110(48), E4581–E4590. https://doi.org/10.1073/pnas.1316830110

Fan, J., Ovtchinnikov, M., Comstock, J. M., McFarlane, S. A., & Khain, A. (2009). Ice formation in Arctic mixed-phase clouds: Insights from a 3-D cloud-resolving model with size-resolved aerosol and cloud microphysics. *Journal of Geophysical Research*, *114*, D04205. https://doi.org/10.1029/2008JD010782

Fierro, A. O., Leslie, L., Mansell, E., Straka, J., MacGorman, D., & Ziegler, C. (2007). A high-resolution simulation of microphysics and electrification in an idealized hurricane-like vortex. *Meteorology and Atmospheric Physics*, *98*(1–2), 13–33. https://doi.org/10.1007/s00703-006-0237-0

Fritsch, J. M., & Carbone, R. E. (2004). Improving quantitative precipitation forecasts in the warm season: A USWRP research and development strategy. *Bulletin of the American Meteorological Society*, *85*(7), 955–965. https://doi.org/10.1175/BAMS-85-7-955

Hazra, A., Mukhopadhyay, P., Taraphdar, S., Chen, J. P., & Cotton, W. R. (2013). Impact of aerosols on tropical cyclones: An investigation using convection-permitting model simulation. *Journal of Geophysical Research: Atmospheres*, *118*, 7157–7168. https://doi.org/10.1002/jgrd.50546

Igel, A. L., & van den Heever, S. C. (2014). Aerosol impacts in shallow convection as simulated by bin and bulk schemes in RAMS. In *The 94th American Meteorological Society Annual Meeting* (pp. 2–6). Atlanta, GA: AMS.

Iguchi, T., Matsui, T., Tao, W. K., Khain, A. P., Phillips, V. T. J., Kidd, C., … Hou, A. (2014). WRF–SBM simulations of melting-layer structure in mixed-phase precipitation events observed during LPVEx. *Journal of Applied Meteorology and Climatology*, *53*(12), 2710–2731. https://doi.org/10.1175/JAMC-D-13-0334.1

Jenkins, G. S., & Pratt, A. (2008). Saharan dust, lightning and tropical cyclones in the eastern tropical Atlantic during NAMMA-06. *Geophysical Research Letters*, *35*, L12804. https://doi.org/10.1029/2008GL033979

Jenkins, G. S., Pratt, A. S., & Heymsfield, A. (2008). Possible linkages between Saharan dust and tropical cyclone rain band invigoration in the eastern Atlantic during NAMMA-06. *Geophysical Research Letters*, *35*, L08815. https://doi.org/10.1029/2008GL034072

Jiang, B., Huang, B., Lin, W., & Xu, S. (2016). Investigation of the effects of anthropogenic pollution on typhoon precipitation and microphysical processes using WRF-Chem. *Journal of the Atmospheric Sciences*, *73*(4), 1593–1610. https://doi.org/10.1175/JAS-D-15-0202.1

Kain, J. S. (1993). Convective parametrization for mesoscale models: The Kain-Fritsch scheme. *Meteorological Monographs*, *46*, 165–170. https://doi.org/10.1007/978-1-935704-13-3_16

Kessler, E. (1969). On the distribution and continuity of water substance in atmospheric circulations. *Meteorological Monographs*, *32*. https://doi.org/10.1007/978-1-935704-36-2

Khain, A., Lynn, B., & Dudhia, J. (2010). Aerosol effects on intensity of landfalling hurricanes as seen from simulations with the WRF model with spectral bin microphysics. *Journal of the Atmospheric Sciences*, *67*(2), 365–384. https://doi.org/10.1175/2009JAS3210.1

Khain, A., Lynn, B., & Shpund, J. (2016). High resolution WRF simulations of Hurricane Irene: Sensitivity to aerosols and choice of microphysical schemes. *Atmospheric Research*, *167*, 129–145. https://doi.org/10.1016/j.atmosres.2015.07.014

Khain, A., Pokrovsky, A., Pinsky, M., Seifert, A., & Phillips, V. (2004). Simulation of effects of atmospheric aerosols on deep turbulent convective clouds using a spectral microphysics mixed-phase cumulus cloud model. Part I: Model description and possible applications. *Journal of the Atmospheric Sciences*, *61*(24), 2963–2982. https://doi.org/10.1175/JAS-3350.1

Khain, A. P. (1984). *Mathematical modeling of tropical cyclones* (247 pp.). St. Petersburg, Russia: Gidrometeoizdat.

Khain, A. P. (2009). Notes on state-of-the-art investigations of aerosol effects on precipitation: A critical review. *Environmental Research Letters*, *4*(1), 015004. https://doi.org/10.1088/1748-9326/4/1/015004

Khain, A. P., BenMoshe, N., & Pokrovsky, A. (2008). Factors determining the impact of aerosols on surface precipitation from clouds: An attempt at classification. *Journal of the Atmospheric Sciences*, *65*(6), 1721–1748. https://doi.org/10.1175/2007JAS2515.1

Khain, A. P., Leung, L. R., Lynn, B., & Ghan, S. (2009). Effects of aerosols on the dynamics and microphysics of squall lines simulated by spectral bin and bulk parameterization schemes. *Journal of Geophysical Research*, *114*, D22203. https://doi.org/10.1029/2009JD011902

Khain, A. P., Beheng, K. D., Heymsfield, A., Korolev, A., Krichak, S. O., Levin, Z., … Yano, J. I. (2015). Representation of microphysical processes in cloud-resolving models: Spectral (bin) microphysics versus bulk parameterization. *Reviews of Geophysics*, *53*, 247–322. https://doi.org/10.1002/2014RG000468

Krall, G. M., & Cottom, W. R. (2012). Potential indirect effects of aerosol on tropical cyclone intensity: Convective fluxes and cold-pool activity. *Atmospheric Chemistry and Physics*, *12*(1), 351–385. https://doi.org/10.5194/acpd-12-351-2012

Lau, W. K., & Kim, K. M. (2007). How nature foiled the 2006 hurricane forecasts. *Eos, Transactions AGU*, *88*(9), 105–107. https://doi.org/10.1029/2007EO090002

Li, G., Wang, Y., Lee, K. H., Diao, Y., & Zhang, R. (2008). Increased winter precipitation over the North Pacific from 1984–1994 to 1995–2005 inferred from the Global Precipitation Climatology Project. *Geophysical Research Letters*, *35*, L13821. https://doi.org/10.1029/2008GL034668

Li, Q., & Wang, Y. (2012). A comparison of inner and outer spiral rainbands in a numerically simulated tropical cyclone. *Monthly Weather Review*, *140*(9), 2782–2805. https://doi.org/10.1175/MWR-D-11-00237.1

Li, Z., Lau, W. K. M., Ramanathan, V., Wu, G., Ding, Y., Manoj, M. G., … Brasseur, G. P. (2016). Aerosol and monsoon climate interactions over Asia. *Reviews of Geophysics*, *54*, 866–929. https://doi.org/10.1002/2015RG000500

Lynn, B., & Khain, A. (2007). Utilization of spectral bin microphysics and bulk parameterization schemes to simulate the cloud structure and precipitation in a mesoscale rain event. *Journal of Geophysical Research*, *112*, D22205. https://doi.org/10.1029/2007JD008475

Lynn, B. H., Khain, A. P., Bao, J. W., Michelson, S. A., Yuan, T., Kelman, G., & Benmoshe, N. (2016). The sensitivity of Hurricane Irene to aerosols and ocean coupling: Simulations with WRF spectral bin microphysics. *Journal of the Atmospheric Sciences*, *73*(2), 467–486. https://doi.org/10.1175/JAS-D-14-0150.1

Lynn, B. H., Khain, A. P., Dudhia, J., Rosenfeld, D., Pokrovsky, A., & Seifert, A. (2005a). Spectral (bin) microphysics coupled with a mesoscale model (MM5). Part I: Model description and first results. *Monthly Weather Review*, *133*(1), 44–58. https://doi.org/10.1175/MWR-2840.1

Lynn, B. H., Khain, A. P., Dudhia, J., Rosenfeld, D., Pokrovsky, A., & Seifert, A. (2005b). Spectral (bin) microphysics coupled with a mesoscale model (MM5). Part II: Simulation of a CAPE rain event with a squall line. *Monthly Weather Review*, *133*(1), 59–71. https://doi.org/10.1175/MWR-2841.1

Ming, J., Zhang, J. A., & Rogers, R. F. (2015). Typhoon kinematic and thermodynamic boundary layer structure from dropsonde composites. *Journal of Geophysical Research: Atmospheres*, *120*(8), 3158–3172. https://doi.org/10.1002/2014JD022640

Ming, J., Shu, S., Wang, Y., Tang, J., & Chen, J. (2012). Modeling rapid intensification of typhoon Saomai (2006) with the weather research and forecasting model and sensitivity to cloud microphysical parameterizations. *Journal of the Meteorological Society of Japan Ser. II*, *90*(5), 771–789. https://doi.org/10.2151/jmsj.2012-513

Pruppacher, H. R., & Klett, J. D. (1997). *Microphysics of clouds and precipitation*. Dordrecht, Netherlands: Kluwer Academy.

Rosenfeld, D., Clavner, M., & Nirel, R. (2011). Pollution and dust aerosols modulating tropical cyclones intensities. *Atmospheric Research*, *102*(1–2), 66–76. https://doi.org/10.1016/j.atmosres.2011.06.006

Rosenfeld, D., Woodley, W. L., Khain, A., Cotton, W. R., Carrió, G., Ginis, I., & Golden, J. H. (2012). Aerosol effects on microstructure and intensity of tropical cyclones. *Bulletin of the American Meteorological Society*, *93*(7), 987–1001. https://doi.org/10.1175/BAMS-D-11-00147.1

Rosenfeld, D., Lohmann, U., Raga, G. B., O'Dowd, C. D., Kulmala, M., Fuzzi, S., … Andreae, M. O. (2008). Flood or drought: How do aerosols affect precipitation? *Science*, *321*(5894), 1309–1313. https://doi.org/10.1126/science.%20110606

Skamarock, W. C., Klemp, J. B., Dudhia, J., Gill, D. O., Barker, D. M., Duda, M. G., … Powers, J. G. (2008). A description of the Advanced Research WRF version 3. NCAR Tech (Note NCAR/TN-4751STR, 113 pp.).

Stoelinga, M. T., Hobbs, P. V., Mass, C. F., Locatelli, J. D., Colle, B. A., Houze, R. A. Jr., … Colman, B. R. (2003). Improvement of microphysical parameterization through observational verification experiment, *Bulletin of the American Meteorological Society*, *84*(12), 1807–1826. https://doi.org/10.1175/BAMS-84-12-1807

Sui, C. H., Li, X., & Yang, M. J. (2007). On the definition of precipitation efficiency. *Journal of the Atmospheric Sciences*, *64*(12), 4506–4513. https://doi.org/10.1175/2007JAS2332.1

Takemura, T., Nakajima, T., Dubovik, O., Holben, B. N., & Kinne, S. (2002). Single-scattering albedo and radiative forcing of various aerosol species with a global three-dimensional model. *Journal of Climate*, *15*(4), 333–352. https://doi.org/10.1175/1520-0442(2002)015%3C0333:SSAARF%3E2.0.CO;2

Takemura, T., Nozawa, T., Emori, S., Nakajima, T. Y., & Nakajima, T. (2005). Simulation of climate response to aerosol direct and indirect effects with aerosol transport-radiation model. *Journal of Geophysical Research*, *110*, D02202. https://doi.org/10.1029/2004JD005029

Takemura, T., Okamoto, H., Maruyama, Y., Numaguti, A., Higurashi, A., & Nakajima, T. (2000). Global three-dimensional simulation of aerosol optical thickness distribution of various origins. *Journal of Geophysical Research*, *105*, 17,853–17,873. https://doi.org/10.1029/2000JD900265

Tao, W. K., Chen, J. P., Li, Z., Wang, C., & Zhang, C. (2012). Impact of aerosols on convective clouds and precipitation. *Reviews of Geophysics*, *50*, RG2001. https://doi.org/10.1029/2011RG000369

Tao, W. K., Li, X., Khain, A., Matsui, T., Lang, S., & Simpson, J. (2007). Role of atmospheric aerosol concentration on deep convective precipitation: Cloud-resolving model simulations. *Journal of Geophysical Research*, *112*, D24S18. https://doi.org/10.1029/2007JD008728

Thompson, G., Field, P. R., Hall, W. D., & Rasmussen, R. M. (2006). A new bulk microphysical parameterization for WRF (& MM5). Presented at the Proceedings of the 7th Weather Research and Forecasting Model Workshop (pp. 1–11). Boulder, CO: NCAR Mesoscale and Microscale Meteorology Division.

Wang, Y. (2009). How do outer spiral rainbands affect tropical cyclone structure and intensity? *Journal of the Atmospheric Sciences*, *66*(5), 1250–1273. https://doi.org/10.1175/2008JAS2737.1

Wang, Y., Zhang, R., & Saravanan, R. (2014). Asian pollution climatically modulates mid-latitude cyclones following hierarchical modelling and observational analysis. *Nature Communications*, *5*, 5836. https://doi.org/10.1038/ncomms4098

Yang, M. J., & Ching, L. (2005). A modeling study of Typhoon Toraji (2001). Physical parameterization sensitivity and topographic effect. *Terrestrial, Atmospheric and Oceanic Sciences*, *16*(1), 177–213. https://doi.org/10.3319/TAO.2005.16.1.177(A)

Yin, Y., Levin, Z., Reisin, T., & Tzivion, S. (2000). Seeding convective clouds with hygroscopic flares: Numerical simulations using a cloud model with detailed microphysics. *Journal of Applied Meteorology*, *39*(9), 1460–1472. https://doi.org/10.1175/1520-0450(2000)039%3C1460:SCCWHF%3E2.0.CO;2

Yu, D. (2015). Intuitionistic fuzzy theory based typhoon disaster evaluation in Zhejiang Province, China: A comparative perspective. *Natural Hazards*, *75*(3), 2559–2576. https://doi.org/10.1007/s11069-014-1450-7

Zhang, H., McFarquhar, G. M., Cotton, W. R., & Deng, Y. (2009). Direct and indirect impacts of Saharan dust acting as cloud condensation nuclei on tropical cyclone eyewall development. *Geophysical Research Letters*, *36*, L06802. https://doi.org/10.1029/2009GL037276

Zhang, Q., Liu, Q., & Wu, L. (2009). Tropical cyclone damages in China 1983–2006. *Bulletin of the American Meteorological Society*, *90*(4), 489–495. https://doi.org/10.1175/2008BAMS2631.1

Zhang, R., Li, G., Fan, J., Wu, D. L., & Molina, M. J. (2007). Intensification of Pacific storm track linked to Asian pollution. *Proceedings of the National Academy of Sciences of the United States of America*, *104*(13), 5295–5299. https://doi.org/10.1073/pnas.0700618104